RESEARCH

Simple synthesis and characterization of $Cs_{0.3}WO_{3.15}/Cs_3PW_{12}O_{40}$ composite for fast adsorption of cationic dyes from water

Nemat Tahmasebi[1] · Zahra Zadehdabagh[1]

Abstract

In this study, cesium-based polyoxometalate compounds ($Cs_{0.3}WO_{3.15}/Cs_3PW_{12}O_{40}$) were successfully synthesized by a simple thermal decomposition method. The effect of phosphoric acid within reaction solution on the phase-change from hexagonal cesium tungstate ($Cs_{0.3}WO_{3.15}$) to Keggin-type polyoxometalate ($Cs_3PW_{12}O_{40}$) and a novel $Cs_{0.3}WO_{3.15}/Cs_3PW_{12}O_{40}$ composite formation were investigated. The products were characterized by XRD, FTIR, FESEM, EDS, DRS, and nitrogen adsorption-desorption isotherms. The powder samples were applied as adsorbent to remove the dye molecules from water. Results indicated that the $Cs_{0.3}WO_{3.15}/Cs_3PW_{12}O_{40}$ composite exhibits higher adsorption capability toward cationic dyes compared with pure $Cs_{0.3}WO_{3.15}$ and $Cs_3PW_{12}O_{40}$. The calculated surface area of pure composite was $\sim 32.079 \, m^2/g$, which is larger than that of pure cesium tungstate ($\sim 17.267 \, m^2/g$). The kinetics and isotherms for RhB adsorption on $Cs_{0.30}WO_{3.15}/Cs_{0.30}WO_{3.15}$ composite were also studied in details.

Keywords Cesium tungstate · Polyoxometalate · Composite · Dye adsorption · Langmuir

Introduction

In recent years, with the development of science and technology, the release of organic dyes into water has been considered as a serious environmental problem [1–4]. Most of the dyes which are stable under light, heat, and other conditions can cause skin irritation, dermatitis, and mutagenic changes in aquatic systems [5–7]. Therefore, the removal of them from wastewater is essential. Up to now, many physical and chemical purification techniques such as photodegradation, oxidation, electrolysis, membrane separation, and adsorption have been applied to remove the contaminants from water [8–13]. Among these methods, adsorption is considered as an efficient, versatile, and cost-effective method [14–16]. Many types of materials including clay mineral, activated carbon, and zeolite have been studied for water treatment [17–19]. Among them, the activated carbon is more widely used as

an adsorbent for removal of water contaminations [20–22]. However, some properties of activated carbon such as high cost, high regeneration temperature, and nonselective restrict its desirability for practical application [1, 7]. Therefore, the further research is needed to develop the more efficient adsorbent with fast adsorption rate for eliminating the organic dyes from wastewater.

Recently, the metal oxides such as TiO_2, WO_3, Fe_2O_3, ZnO, and ZrO_2 have been widely investigated as adsorbents to eliminate the dyes from wastewater because of unique physical properties, low cost, and environmentally friendly nature [23–27]. Polyoxometalates are one of the most outstanding metal oxides with controllable size and morphology and highly negatively charged surface, which can be used as an excellent adsorbent for selective removal of cationic dyes from waste water compared to anionic dyes due to electrostatic interaction between dyes and polyoxometalate surface [28–30]. In recent years, these compounds have attracted much research interest in many other areas such as catalysts, electrochemistry, and sensors due to unique physical and chemical properties [31, 32]. Among the various polyoxometalates, cesium-based polyoxometalates, $Cs_3PW_{12}O_{40}$, which are insoluble in water are considered as a good candidate for catalytic reactions in liquid phase

✉ Nemat Tahmasebi
tahmasebi@jsu.ac.ir

1   Department of Physics, Jundi-Shapur University of Technology, Dezful, Iran

Fig. 1 XRD patterns of synthesized samples using different amounts of phosphoric acid within reaction solution (S1) 0 ml, (S2) 10 ml, (S3) 15 ml, and (S4) 20 ml
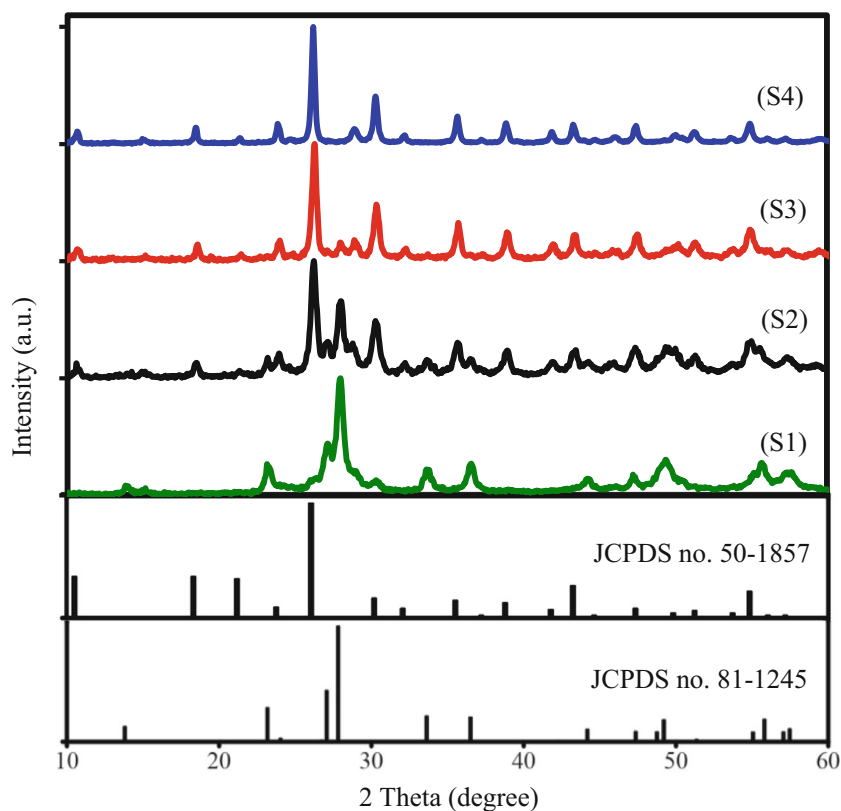
because of their excellent photochemical characteristic such as high surface area and evolved porosity [32–34]. However, the dye adsorption properties of $Cs_3PW_{12}O_{40}$-based compound rarely have been investigated.

In this study, we report the phase-change from hexagonal cesium tungstate ($Cs_{0.3}WO_{3.15}$) to Keggin-type polyoxometalate ($Cs_3PW_{12}O_{40}$) and a novel $Cs_{0.3}WO_{3.15}$/$Cs_3PW_{12}O_{40}$ composite formation by a simple thermal decomposition method with the assistant of phosphoric acid. The X-ray diffraction (XRD), Fourier transform microscopy (FTIR), scanning electron microscopy (SEM), and UV-vis

diffuse reflectance spectroscopy (DRS) were used to characterize the products. The dye adsorption capabilities of synthesized samples were investigated by the adsorption of RhB from water at room temperature. The adsorption kinetics and the adsorption isotherms were also studied in details.

Experimental

Tungstic acid (H_2WO_4), cesium carbonate (Cs_2CO_3) and polyvinylpyrrolidone (PVP, Mw = 1,300,000), rhodamine B (RhB), malachite green (MG), methyl orange (MO), and methylene blue (MB) were purchased from Sigma-Aldrich corporation. All reagents were of analytical grade and used as received without further purification. In this study, the products were synthesized by using a simple and scale able thermal decomposition method. As a typical, 0.751 g of H_2WO_4 was dissolved in 5 ml of hydrogen peroxide (H_2O_2) at 50 °C. After magnetic stirring for 1 h, 2.5 ml ammoniac (NH_3), 2 g citric acid, and different amounts of phosphoric acid (H_3PO_4, 10 mM) were added into the above solution to form a transparent solution under magnetic stirring for 30 min. The amount of phosphoric acid was set to be 0, 10 ml, 15 ml, and 20 ml. Then, 0.153 g cesium carbonate was added into the solution with continuous stirring for 30 min. After that, certain amount of PVP (27% molar weight of solution) was added into the mixed solution and the solution was stirred for 8 h at room
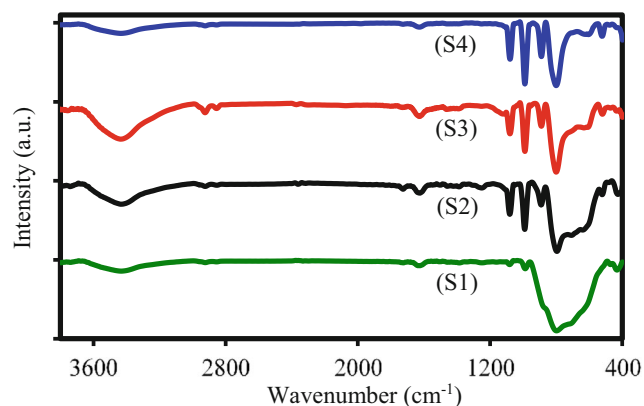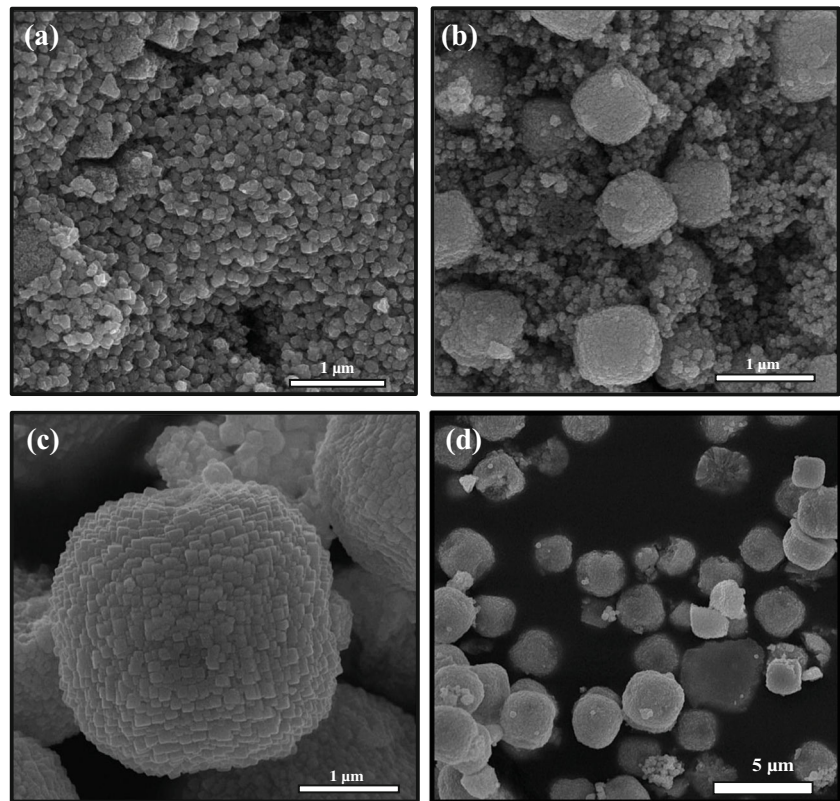

Fig. 2 FT-IR spectra of synthesized samples using different amounts of phosphoric acid within reaction solution (S1) 0 ml, (S2) 10 ml, (S3) 15 ml, and (S4) 20 ml

Fig. 3 SEM images of **a** S1, **b** S2, and **c**–**d** S4 samples

temperature. The obtain sol was thermal decomposed at 500 °C for 2 h with heating rate of 1 °C min^{-1}. The as-prepared powder was washed with deionized water for three times and finally dried at 70 °C for 6 h. The synthesized samples with the adding of 0, 10 ml, 15 ml, and 20 ml phosphoric acid into reaction solution are labeled as S1, S2, S3, and S4, respectively.

The morphology of synthesized powder samples were specified by field emission scanning electron microscopy (FESEM) using a TESCAN-Mirri III, equipped with an energy dispersive x-ray spectroscopy (EDS). The crystal structure of products was determined by x-ray diffraction pattern
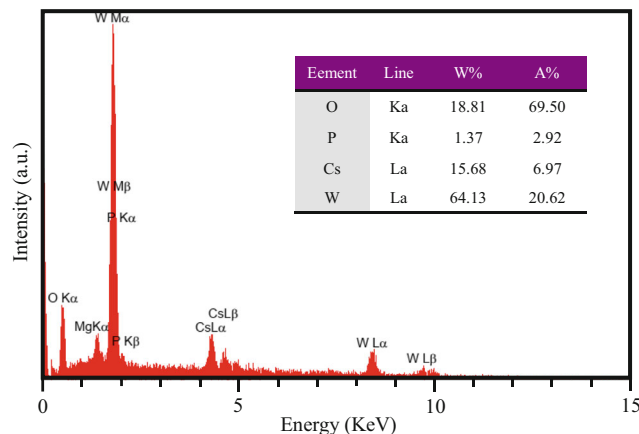
(XRD, PHILIPS- PW1730) with a Cu Kα radiation (λ = 1.54056 Å) operated at 40 kV and 30 mA. To confirm the Keggin structure formation, Fourier transform infrared (FTIR) spectra of the samples were recorded at room temperature using a Thermo-Avatar in the range 4000–400 cm^{-1}. UV-vis diffuse reflectance spectroscopy (DRS) was recorded on an Avaspec-2048-TEC spectrometer using $BaSO_4$ as a reference in the wavelength range of 200–800 nm. The specific surface area values were calculated from nitrogen adsorption-

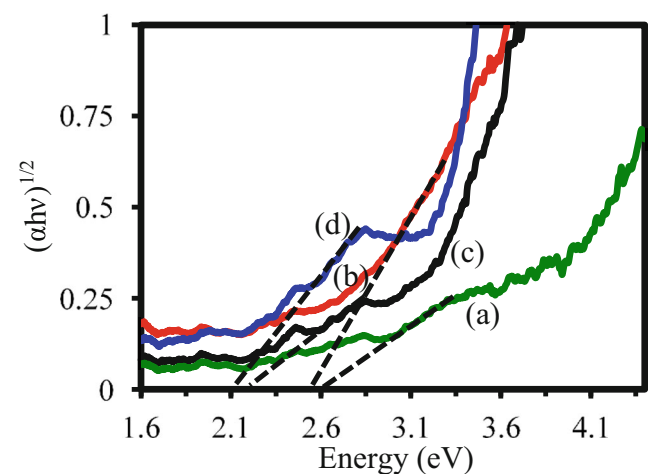| Eement	Line	W%	A%
O	Ka	18.81	69.50
P	Ka	1.37	2.92
Cs	La	15.68	6.97
W	La	64.13	20.62

Fig. 4 EDS analysis of S2 sample

Fig. 5 UV-vis DRS spectra and corresponding band gap energy of **a** S1, **b** S2, **c** S3, **d** S4 samples
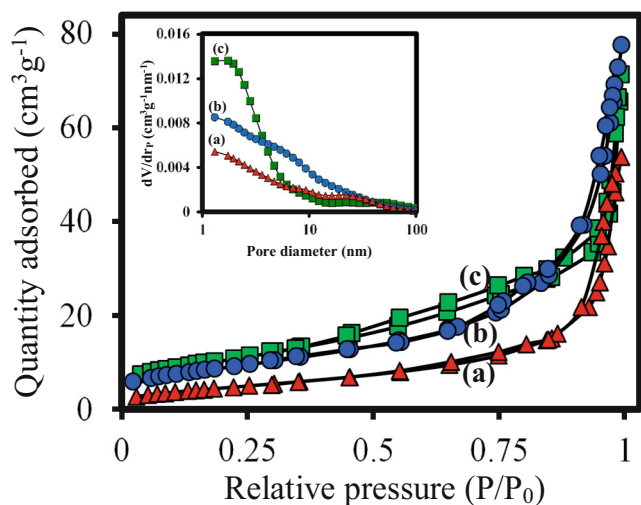
Fig. 6 N_2 adsorption/desorption of **a** S1, **b** S2, and **c** S4 samples

desorption isotherms obtained at 77 K using a BELSORP MINI II analyzer.

To do the adsorption experiment, 40 mg of the powder samples was added into 40 ml RhB (10 mg/l) aqueous solution under stirring in dark. Then, the powder samples were removed by centrifugation and the remaining concentration of RhB was measured using UV-vis spectrophotometer. The percent removal of dyes from aqueous solution was determined by the following equation:

$$\%Removal = \frac{C_0 - C_e}{C_0} \times 100 \qquad (1)$$

where C_0 and C_e are the initial and final concentration (mg/L) of the dyes, respectively. Furthermore, the adsorption amount (mg/g) at different times was calculated as below:

$$q_t = \frac{(C_0 - C_t) \times V}{m} \qquad (2)$$

where C_0 and C_t are the concentration of dye (mg/L) at initial time and at different times, respectively, V (L) is the volume of dye solution and m (g) is the amount of adsorbent.

Results and discussion

The phase structure of products was characterized by x-ray diffraction (XRD) analysis. Figure 1 shows the XRD patterns

of synthesized samples by simple thermal decomposition method using different amounts of phosphoric acid within reaction solution. It is observed that all the diffraction peaks of synthesized sample in the absence of phosphoric acid can well be assigned to hexagonal phase of cesium tungstate ($Cs_{0.30}WO_{3.15}$, JCPDS no. 81-1245) with the crystal lattice parameters of a = 7.4012 Å, b = 7.4012 Å, and c = 7.6728 Å, indicating single phase of $Cs_{0.30}WO_{3.15}$ was formed. When small amount of phosphoric acid was added into reaction solution, the XRD pattern of sample displays the coexistence of cesium tungstate and cesium polyoxometalates ($Cs_3PW_{12}O_{40}$, JCPDS no. 50-1857) phases, which suggests the $Cs_{0.30}WO_{3.15}/Cs_{0.30}WO_{3.15}$ composite formation. As shown in Fig. 1, the intensity of diffraction peaks corresponding to $Cs_3PW_{12}O_{40}$ increases with increasing phosphoric acid content, while the intensity of $Cs_{0.30}WO_{3.15}$ peaks has decreased. However, it is observed when 20 ml of phosphoric acid was added into reaction solution, all the diffraction peaks nearly can be indexed to the $Cs_3PW_{12}O_{40}$, indicating that pure $Cs_3PW_{12}O_{40}$ has been formed.

The FT-IR spectra of S1, S2, S3, and S4 samples are presented in Fig. 2. The S1 sample displays a broad absorption band in the range of 540–950 cm^{-1}, which can be attribute to the oxygen-tungsten bonds [35, 36]. When small amount of phosphoric acid was added into reaction solution, the absorption bands at 1078, 990, 880, 798, and 520 cm^{-1} have been appeared. As previously reported, the characteristic bands of Kegging type polyoxometalates observed at 1078, 983, 887, 793, and 524 cm^{-1} belong to the vibration of the P–O bonds of PO_4 units, W=O bonds, corner-sharing and edge-sharing vibration of W–O–W bonds, and symmetric vibration of O–P–O, respectively [37, 38]. These results confirm the Keggin-type structure formation in the presence of phosphoric acid within reaction solution. Moreover, the intensity of characteristic peaks of $Cs_3PW_{12}O_{40}$ has increased with increasing phosphoric acid content.

The morphology and particle size distribution of the products were characterized by FESEM analysis. Figure 3 displays the FESEM images of synthesized samples in the presence of different contents of phosphoric acid within reaction solution. It is observed the pure $Cs_{0.3}WO_{3.15}$ (S1 sample) is composed of nearly uniform nanoparticles with the average size of ~ 70 nm. As shown in Fig. 3b, in the presence of small amount of phosphoric acid, in addition to $Cs_{0.3}WO_{3.15}$ nanoparticles, microspheres with the diameter of around 1 μm are also observed. Based on XRD analysis which indicated that this

Table 1 BET surface area, total pore volume, and mean pore diameter of S1, S2, and S4 samples

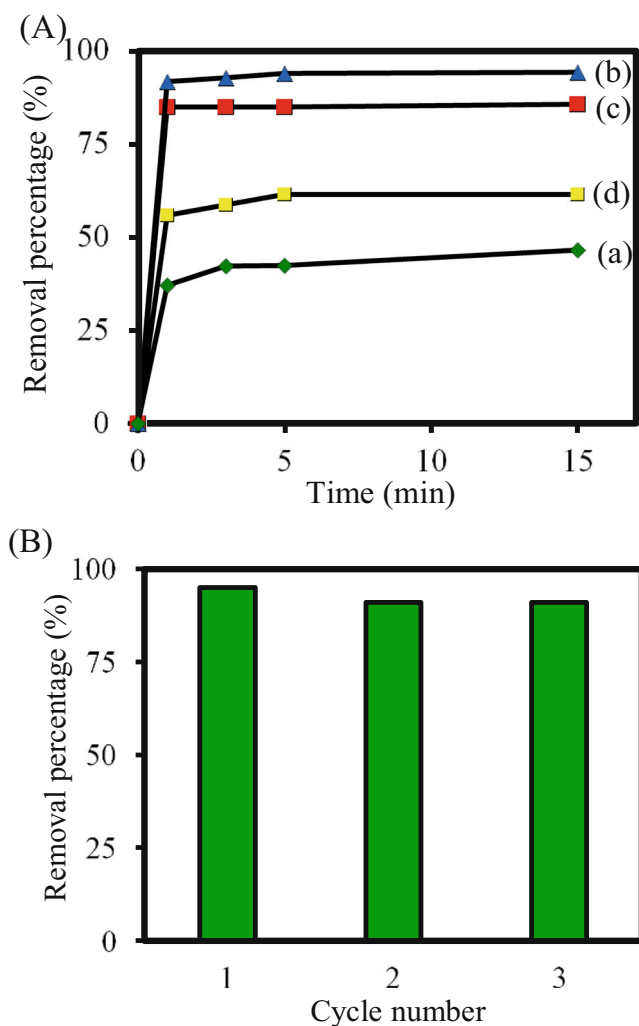| Sample	Surface area ($m^2 \ g^{-1}$)	Total pore volume ($cm^3 \ g^{-1}$)	Mean pore diameter (r_p-nm)
(a)	17.267	0.0813	18.836
(b)	32.079	0.1164	14.519
(c)	37.943	0.1034	10.904

(A)

(B)

Fig. 7 (A) The removal efficiency of synthesized samples using different amounts of phosphoric acid for removal of RhB from water: (a) S1, (b) S2, (c) S3, and (d) S4, and (B) Removal efficiency of MB onto S2 in three successive cycles.

sample is composed of a two-phase structure, the observed microspheres can be attributed to the $Cs_3PW_{12}O_{40}$ compound. Moreover, the size and the number of the microspheres increase with increasing phosphoric acid content. It can be seen the synthesized sample with 20 ml H_3PO_4 content (Fig. 3c–d) is composed of nearly uniform microspheres with the average diameter size of ~ 2 μm, which confirms that nearly all of the $Cs_{0.3}WO_{3.15}$ nanoparticles have transformed into $Cs_3PW_{12}O_{40}$. Interestingly, the microspheres are composed of nanoparticles with the size of ~ 90 nm. The chemical composition of the products was determined by energy dispersive x-ray spectroscopy (EDS) analysis. As a typical, Fig. 4 displays the EDS spectrum of S2 composite sample. It is observed this sample is composed of O, Cs, W, and P elements, which confirm the purity of products.

The UV-vis diffuse reflectance spectroscopy (DRS) was used to investigate the optical properties of products. Based on DRS spectra, the band gap (E_g) of samples is determined

by extrapolating and intersecting the linear part of $(\alpha h v)^{1/2}$ to $h v$-axis. Where, α is the optical absorption coefficient and $h v$ is photon energy. As shown in Fig. 5, the band gap of S1, S2, S3, and S4 samples is estimated to be nearly 2.60 eV, 2.52 eV, 2.25 eV, and 2.20 eV, respectively. Thus, the band gap of samples exhibits a red-shift with increasing phosphor content, which confirms the phase changes from hexagonal cesium tungstate ($Cs_{0.3}WO_{3.15}$) to Keggin-type polyoxometalate ($Cs_3PW_{12}O_{40}$).

It is well known that the adsorption capacity of an adsorbent can be controlled by its specific surface area. A larger specific surface area can provide more active sites for surface adsorption of dye molecules [39]. The N_2 adsorption-desorption isotherms were applied to determine the surface area, total pore volume, and mean pore diameter of S1, S2, and S4 samples. As shown in Fig. 6, all samples display type IV isotherms with a H_3 hysteresis loop, indicating the presence of mesoporous structure [40]. The pore structural properties of the samples are represented in Table 1. It is observed the specific surface areas calculated by BET method are 17.26 m^2/g, 32.07 m^2/g, and 37.94 m^2/g for S1, S2, and S4 samples, respectively.

The adsorption capability of samples was studied by the adsorption of RhB in water under dark condition. In each experiment, 40 mg of powder samples was added into 40 ml RhB aqueous solution (10 ppm). Figure 7A shows the adsorption performance of S1, S2, S3, and S4 samples for adsorption removal of RhB from water as a function of contact times. It is observed all the samples display a rapid adsorption process in the first 1 min, which exhibits the availability of active surface sites [20]. The adsorption percentage of S1, S2, S3, and S4 samples toward RhB in aqueous solution was 46%, 95%, 85%, and 61%, respectively, demonstrating that the adsorption capacity of composite is larger than other samples.

Furthermore, the reusability of an adsorbent is important for practical applications. In each experiment, after RhB adsorption, the powder was separated by centrifugation and washed with distilled water and ethanol, and then dried in an oven at 80 °C for the next test. Figure 7B shows the stability of S2 toward the removal of RhB from aqueous solution for three consecutive cycles. It is observed the adsorption performance slightly decreased from 95 to 91% after three cycles, indicating the good stability.

Furthermore, the selective adsorption performance of S2 sample toward MB, MG, and RhB as cationic dyes and MO as an anionic dye was evaluated. Figure 8 displays the changes of UV-vis absorption spectra of dye solution (40 ml, 10 mg/L) before and after addition of composite sample (40 mg) as adsorbent under dark condition for 20 min. It is observed, the dye adsorption toward MB, MG, and RhB as cationic dyes is > 95%,
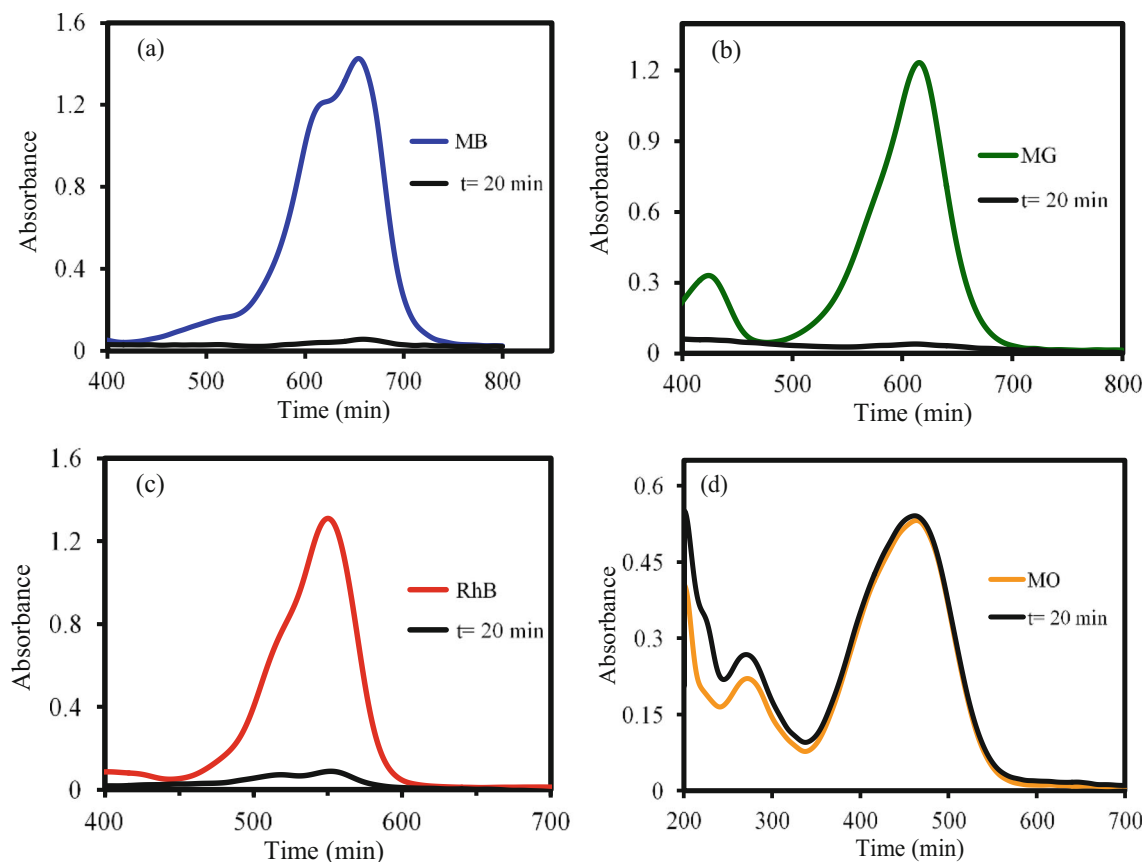
Fig. 8 UV-vis absorption spectra of dye solution (40 ml, 10 mg/L) before and after addition of S2 samples (40 mg) under dark condition for 20 min

whereas the amount of adsorbed MO as an anionic dye onto the sample is negligible. These results imply that the composite sample has an excellent adsorption capability toward cationic dyes, whereas displays no adsorption toward MO as an anionic dye.

To describe the adsorption process onto composite samples two kinetic models, pseudo-first order (Eq. 3) and pseudo-second order (Eq. 4), were fitted to experimental data. These models can be expressed as below [40–42]:

$$\ln(q_e - q_t) = \ln q_e - k_1 t \tag{3}$$

$$\frac{t}{q_t} = \frac{1}{k_2 q_e^2} + \frac{t}{q_e} \tag{4}$$

where q_e (mg/g) is the amount of RhB adsorbed at equilibrium and q_t (mg/g) is the amount of RhB adsorbed at various time; t is the adsorption time and k_1 and k_2 are the first-order and second-order rate constants for RhB adsorption, respectively. These values are determined by linear plots to the experimental data (Fig. 9a, b) and summarized in Table 2. It is observed the correlation coefficient of pseudo second-order model ($R^2 = 0.999$) is much higher than that from pseudo first-order model ($R^2 = 0.664$). Thus, the kinetic of RhB adsorption onto S2 sample was better fitted by pseudo second-order model

compared with pseudo first-order model, indicating the chemical adsorption process is the rate-limiting step [43, 44].

To further determine the adsorption mechanism, the experimental data were fitted by the Langmuir and the Freundlich adsorption isotherm models. The Langmuir and the Freundlich isotherm models describe the monolayer adsorption and multilayer adsorption onto the adsorbent surface, respectively [41, 42]. The linearized form of Langmuir model and the logarithmic form of Freundlich model can be expressed as Eq. 5 and Eq. 6, respectively [41, 42]:

$$\frac{C_e}{q_e} = \frac{1}{q_m K_L} + \frac{C_e}{q_m} \tag{5}$$

$$\text{Log}(q_e) = \text{Log}(K_F) + \frac{1}{n}\text{Log}(C_e) \tag{6}$$

where q_e (mg/g) is the amount of RhB adsorbed at equilibrium, q_m is the maximum adsorption capacity, C_e (mg/L) is the concentration of RhB at equilibrium, K_L is the Langmuir constant, K_f is the Freundlich constant and $1/n$ is the intensity of adsorption. The fitting of both isotherm models to experimental data (Fig. 9c, d), and also corresponding parameters and correlation coefficients for the more are presented in Table 2.
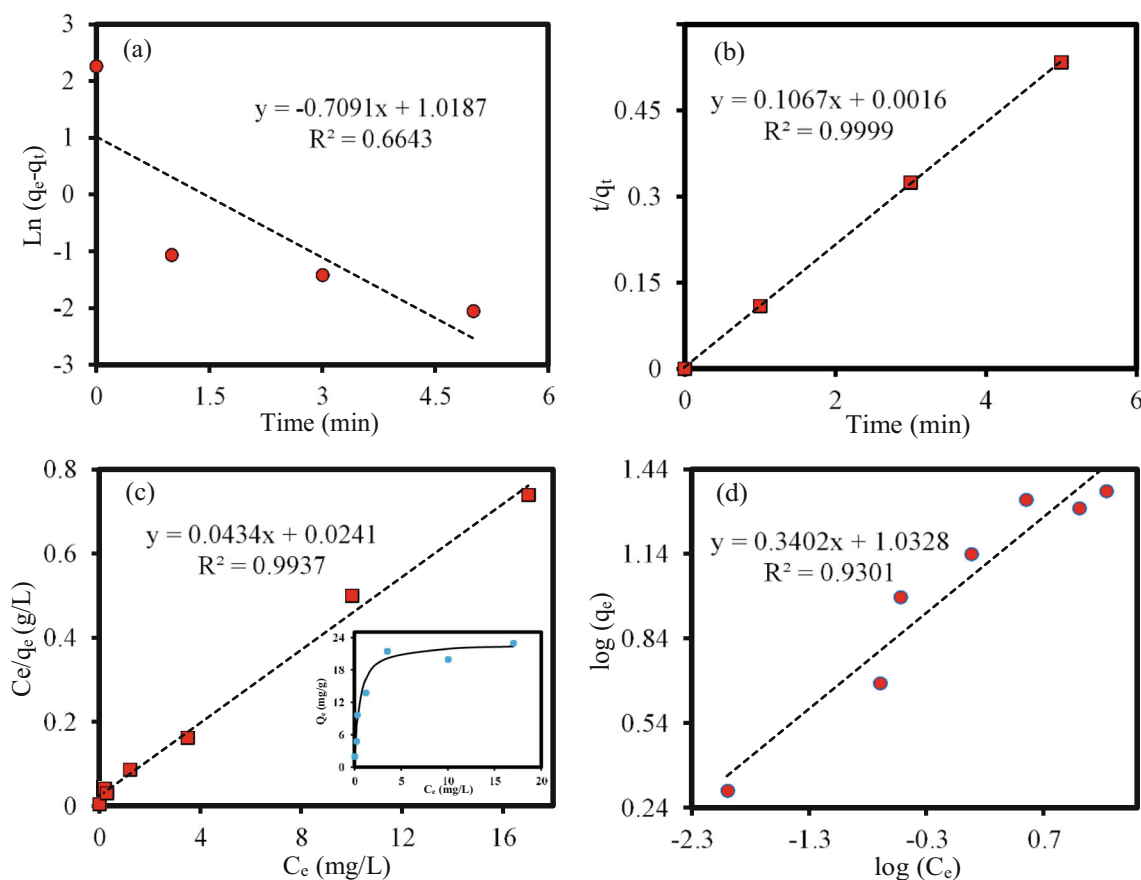
Fig. 9 Fitting adsorption kinetics and isotherms data for RhB on S2 composite sample with **a** pseudo first-order kinetic model, **b** pseudo second-order kinetic model, **c** Langmuir adsorption isotherm (inset: adsorption isotherm of RhB adsorption on composite), and **d** Freundlich adsorption isotherm

It is observed the deviation between the experimental data and fitting curve of the Freundlich model (R^2 = 0.920) is larger than that of the Langmuir model (R^2 = 0.993). In addition, based on the Langmuir model, the value of q_m is ~ 23.041 mg/g, which is in good agreement to the experimental data displayed in the inset of Fig. 9c. Therefore, the adsorption of RhB on the S2 surface obeys the Langmuir adsorption model.

Conclusion

In summary, a simple thermal decomposition method was used to synthesize pure $Cs_{0.3}WO_{3.15}$, $Cs_{0.3}WO_{3.15}$/$Cs_3PW_{12}O_{40}$ composite, and $Cs_3PW_{12}O_{40}$. The results

revealed that the phosphoric acid into reaction solution plays crucial role in the crystal structure and morphology of synthesized samples. It was observed a phase-change from hexagonal cesium tungstate ($Cs_{0.3}WO_{3.15}$) to Keggin-type polyoxometalate ($Cs_3PW_{12}O_{40}$) with the assistance of phosphoric acid. The adsorption experiment indicated that composite sample exhibits a fast and high adsorption performance toward anionic dye (RhB, MB, and MG) compared to pure $Cs_{0.3}WO_{3.15}$ and $Cs_3PW_{12}O_{40}$ phases, whereas its ability to adsorb MO as an anionic dye is negligible. The maximum adsorption capacity of composite sample toward RhB was 23.041 mg/g. The fitting of isotherms and kinetics models to experimental data revealed that the adsorption

Table 2 Kinetic and isotherm parameters for RhB adsorption on S2 sample

	Kinetic						Isotherm					
	First-order			Second-order			Langmuir			Freundlich		
Parameter	k_1	q_e	R^2	k_2	q_e	R^2	q_m	K_L	R^2	K_F	$1/n$	R^2
Value	0.709	2.769	0.664	7.115	9.372	0.999	23.041	2.066	0.993	15.743	0.223	0.920

of RhB on the composite sample was better fitted by Langmuir adsorption model and pseudo second-order model.

References

1. Cramer, A.J., Cole, J.M.: Removal or storage of environmental pollutants and alternative fuel sources with inorganic adsorbents via host–guest encapsulation. J. Mater. Chem. A. **5**, 10746–10771 (2017)

2. Liu, B., Wang, J., Wu, J., Li, H., Li, Z., Zhou, M., Zuo, T.: Controlled fabrication of hierarchical WO_3 hydrates with excellent adsorption performance. J. Mater. Chem. A. **2**, 1947–1954 (2014)

3. Adhikari, S., Mandal, S., Sarkar, D., Kim, D.H., Madras, G.: Kinetics and mechanism of dye adsorption on WO_3 nanoparticles. Appl. Surf. Sci. **420**, 472–482 (2017)

4. Qiao, X.Q., Hu, F.C., Tian, F.Y., Hou, D.F., Li, D.S.: Equilibrium and kinetic studies on MB adsorption by ultrathin 2D MoS_2 nanosheets. RSC Adv. **6**, 11631–11636 (2016)

5. Chen, X., Zhang, F., Wang, Q., Han, X., Li, X., Liu, J., Lin, H., Qu, F.: The synthesis of ZnO/SnO_2 porous nanofibers for dye adsorption and degradation. Dalton Trans. **44**, 3034–3042 (2015)

6. Han, S., Liu, K., Hu, L., Teng, F., Yu, P., Zhu, Y.: Superior adsorption and regenerable dye adsorbent based on flower-like molybdenum disulfide nanostructure. Sci. Rep. **7**, 43599 (2017)

7. Zhao, Z., Ping, N., Di, J., Zheng, H.: Highly selective adsorption of organic dyes onto tungsten trioxide nanowires. Res. Chem. Intermed. **42**, 5639–5651 (2016)

8. Intaphong, P., Phuruangrat, A., Thongtem, T., Thongtem, S.: Effect of pH on phase, morphologies, and photocatalytic properties of BiOCl synthesized by hydrothermal method. J. Aust. Ceram. Soc. (2019). https://doi.org/10.1007/s41779-019-00373-z

9. Forgacs, E., Cserhati, T., Oros, G.: Removal of synthetic dyes from wastewaters: a review. Environ. Int. **30**, 953–971 (2004)

10. Duan, Y., Chen, Y., Wen, Q., Duan, T.: Electrodeposition preparation of a cauliflower-like $Sb–SnO_2$ electrode from DMSO solution for electrochemical dye decolorization. RSC Adv. **6**, 48043–48048 (2016)

11. Hua, M., Zhang, S., Pan, B., Zhang, W., Lv, L., Zhang, Q.: Heavy metal removal from water/wastewater by nanosized metal oxides: a review. J. Hazard. Mater. **211**, 317–331 (2012)

12. Fan, H., Gu, J., Meng, H., Knebel, A.: Caro. J.: High-flux membranes based on the covalent organic framework COF-LZU1 for selective dye separation by nanofiltration. Angew. Chem. Int. Ed. **57**, 4083–4087 (2018)

13. Li, L.H., Xiao, J., Liu, P., Yang, G.W.: Super adsorption capability from amorphousization of metal oxide nanoparticles for dye removal. Sci. Rep. **5**, 9028 (2015)

14. Jeon, S., Yong, K.: Morphology-controlled synthesis of highly adsorptive tungsten oxide nanostructures and their application to water treatment. J. Mater. Chem. **20**, 10146–10151 (2010)

15. Zhang, S., Yang, H., Huang, H., Gao, H., Wang, X., Cao, R., Li, J., Xu, X., Wang, X.: Unexpected ultrafast and high adsorption capacity of oxygen vacancy-rich WO_x/C nanowire networks for aqueous Pb^{2+} and methylene blue removal. J. Mater. Chem. A. **5**, 15913–15922 (2017)

16. Singh, N.B., Nagpal, G., Agrawal, S.: Water purification by using adsorbents: a review. Environ. Technol. Innov. **11**, 187–240 (2018)

17. Auta, M., Hameed, B.H.: Chitosan–clay composite as highly effective and low-cost adsorbent for batch and fixed-bed adsorption of methylene blue. Chem. Eng. J. **237**, 352–361 (2014)

18. Tamai, H., Kakii, T., Hirota, Y., Kumamoto, T., Yasuda, H.: Synthesis of extremely large mesoporous activated carbon and its unique adsorption for giant molecules. Chem. Mater. **8**, 454–462 (1996)

19. Wang, S., Li, H., Xu, L.: Application of zeolite MCM-22 for basic dye removal from wastewater. J. Colloid Interface Sci. **295**, 71–78 (2006)

20. Wang, S., Yang, B., Liu, Y.: Synthesis of a hierarchical SnS_2 nanostructure for efficient adsorption of Rhodamine B dye. J. Colloid Interface Sci. **507**, 225–233 (2017)

21. Crini, G.: Non-conventional low-cost adsorbents for dye removal: a review. Bioresour. Technol. **97**, 1061–1085 (2006)

22. Wang, F., Li, C., Jimmy, C.Y.: Hexagonal tungsten trioxide nanorods as a rapid adsorbent for methylene blue. Sep. Purif. Technol. **91**, 103–107 (2012)

23. Rankin, J.M., Baker, S., Klabunde, K.J.: Mesoporous aerogel titanium oxide–silicon oxide combinations as adsorbents for an azo-dye. Microporous Mesoporous Mater. **190**, 105–108 (2014)

24. Luo, J.Y., Lin, Y.R., Liang, B.W., Li, Y.D., Mo, X.W., Zeng, Q.G.: Controllable dye adsorption behavior on amorphous tungsten oxide nanosheet surfaces. RSC Adv. **5**, 100898–100904 (2015)

25. Maiti, D., Mukhopadhyay, S., Devi, P.S.: Evaluation of mechanism on selective, rapid, and superior adsorption of Congo red by reusable mesoporous α-Fe_2O_3 nanorods. ACS Sustain. Chem. Eng. **5**, 11255–11267 (2017)

26. Ada, K., Ergene, A., Tan, S., Yalçın, E.: Adsorption of remazol brilliant blue R using ZnO fine powder: equilibrium, kinetic and thermodynamic modeling studies. J. Hazard. Mater. **165**, 637–644 (2009)

27. Wang, C., Le, Y., Cheng, B.: Fabrication of porous ZrO_2 hollow sphere and its adsorption performance to Congo red in water. Ceram. Int. **40**, 10847–10856 (2014)

28. Pourzare, K., Farhadi, S., Mansourpanah, Y.: Anchoring $H_3PW_{12}O_{40}$ on aminopropylsilanized spinel-type cobalt oxide (Co_3O_4-$SiPrNH_2$/$H_3PW_{12}O_{40}$): a novel nanohybrid adsorbent for removing cationic organic dye pollutants from aqueous solutions. Appl. Organomet. Chem. **32**, e4341 (2018)

29. Yi, F.Y., Zhu, W., Dang, S., Li, J.P., Wu, D., Li, Y.H., Sun, Z.M.: Polyoxometalates-based heterometallic organic–inorganic hybrid materials for rapid adsorption and selective separation of methylene blue from aqueous solutions. Chem. Commun. **51**, 3336–3339 (2015)

30. Liu, X., Gong, W., Luo, J., Zou, C., Yang, Y., Yang, S.: Selective adsorption of cationic dyes from aqueous solution by polyoxometalate-based metal–organic framework composite. Appl. Surf. Sci. **362**, 517–524 (2016)

31. Meziani, D., Abdmeziem, K., Bouacida, S., Trari, M., Merazig, H.: Photo-electrochemical and physical characterizations of a new single crystal POM-based material. Application to rhodamine B photodegradation. Sol. Energy Mater. Sol. Cells. **147**, 46–52 (2016)

32. Tahmasebi, N., Mirzavand, S., Hakimyfard, A., Barzegar, S.: The excellent photocatalytic activity of novel $Cs_3PW_{12}O_{40}/WO_3$ composite toward the degradation of rhodamine B. Adv. Powder Technol. **30**, 257–265 (2019)

33. Narasimharao, K., Brown, D.R., Lee, A.F., Newman, A.D., Siril, P.F., Tavener, S.J., Wilson, K.: Structure–activity relations in Cs-doped heteropolyacid catalysts for biodiesel production. J. Catal. **248**, 226–234 (2007)

34. Pradhan, S., Mishra, B.G.: $Cs_xH_{3-x}PW_{12}O_{40}$ nanoparticles dispersed in the porous network of Zr-pillared α-zirconium phosphate as efficient heterogeneous catalyst for synthesis of spirooxindoles. Mol. Catal. **446**, 58–71 (2018)

35. Ryu, S.M., Nam, C.: Adsorption characteristics of methylene blue on WO_3 nanorods prepared by microwave-assisted hydrothermal methods. Phys. Stat. Solidi (A). **215**, 1700996 (2018)

36. Huang, X.J., Bao, J., Han, Y., Cui, C.W., Wang, J.X., Zeng, X.F., Chen, J.F.: Controllable synthesis and evolution mechanism of tungsten bronze nanocrystals with excellent optical performance for energy-saving glass. J. Mater. Chem. C. **6**, 7783–7789 (2018)

37. Xiaoxiang, H., Yingying, K., Chunhua, X., Xiujuan, T., Qing, C., Kuiwu, W., Chin-Te, H., Li-Li, L., Shang-Bin, L.: Heteropoly tungstate supported on metal oxide catalysts for liquid phase oxidation of benzyl alcohol with hydrogen peroxide. J. Braz. Chem. Soc. **29**, 88–98 (2018)

38. Yang, H., Liu, X., Sun, S., Nie, Y., Wu, H., Yang, T., Zheng, S., Lin, S.: Green and facile synthesis of graphene nanosheets/$K_3PW_{12}O_{40}$ nanocomposites with enhanced photocatalytic activities. Mater. Res. Bull. **78**, 112–118 (2016)

39. Liu, X., Jin, A., Jia, Y., Xia, T., Deng, C., Zhu, M., Chen, C., Chen, X.: Synergy of adsorption and visible-light photocatalytic degradation of methylene blue by a bifunctional Z-scheme heterojunction of WO_3/g-C_3N_4. Appl. Surf. Sci. **405**, 359–371 (2017)

40. Thommes, M., Kaneko, K., Neimark, A.V., Olivier, J.P., Rodriguez-Reinoso, F., Rouquerol, J., Sing, K.S.W.: Physisorption of gases, with special reference to the evaluation of surface area and pore size distribution (IUPAC Technical Report). Pure Appl. Chem. **87**, 1051–1069 (2015)

41. Sabna, V., Thampi, S.G., Chandrakaran, S.: Degradation of rhodamine B with manganese dioxide nanorods. J. Water Health. **16**, 846–856 (2018)

42. Yang, C., Cheng, J., Chen, Y., Hu, Y.: Enhanced adsorption performance of MoS_2 nanosheet-coated MIL-101 hybrids for the removal of aqueous rhodamine B. J. Colloid Interface Sci. **504**, 39–47 (2017)

43. Massey, A.T., Gusain, R., Kumari, S., Khatri, O.P.: Hierarchical microspheres of MoS_2 nanosheets: efficient and regenerative adsorbent for removal of water-soluble dyes. Ind. Eng. Chem. Res. **55**, 7124–7131 (2016)

44. Ho, Y.S., McKay, G.: Pseudo-second order model for sorption processes. Process Biochem. **34**, 451–465 (1999)